Flotation separation influenced by the rheological properties of diaspore-pyrite mixed pulp

Yongqing Zhao, Xianhai Li

Mining College, Guizhou University, Guiyang 550025, China

National and Local Joint Laboratory of Engineering for Effective Utilization of Regional Mineral Resources from Karst Areas, Guiyang 550025, China

Guizhou Key Lab of Comprehensive Utilization of Non-metallic Mineral Resources, Guizhou University, Guiyang 550025, China

Corresponding author: xhli1@gzu.edu.cn (Xianhai Li)

Abstract: The effects of pyrite and diaspore with different particle sizes on the rheological properties of pulp with butyl xanthate added as a collector were studied, and the mechanism for rheological pyrite separation from diaspore by flotation was probed. The apparent viscosity of the diaspore pulp with different particle sizes was higher than that of pyrite, especially for -30 μm diaspore. Microfine diaspore was an important component affecting the apparent viscosity and yield stress of the diaspore-pyrite mixed pulp, and the pulp became a non-Newtonian fluid when the mass fraction of fine-grained diaspore in the mixed pulp was high. In this study, sodium hexametaphosphate (SHMP) was used to control the rheology of the mixed pulp and improve the pyrite flotation, and the S (sulfur) recovery rate first increased and then decreased with increasing SHMP concentration. The apparent viscosity of the pulp decreased by 3.01% and the S recovery rate increased by 34.83% when the amount of added SHMP was 0.05 mg/kg. The apparent viscosity with 0.50 mg/kg SHMP was 21.76% lower than that seen with the addition of 0.05 mg/kg SHMP, but the S recovery rate was also reduced by 14.94%. Further research showed that the increased SHMP concentration led to increases in the electronegativities of the particle surface and the repulsive force between particles, which prevented agglomeration of the particles, reduced the apparent viscosity and yield stress of the mixed pulp, promoted collisions between the pyrite particles and the bubbles, and reduced the resistance of the air bubbles to flotation.

Keywords: bauxite, diaspore, pyrite; flotation, rheological property, viscosity

1. Introduction

Aluminum alloys are among the most widely used metal materials in the world (Chen et al.,, 2022; Zhang et al., 2023), the second largest metal material after steel, and they are extensively used in the aerospace, construction, chemical and shipbuilding industries (Cheng et al., 2022). There are many aluminum-bearing ores in nature, among which bauxite is the main one with commercial value. Bauxite can be divided into 3 types: gibbsite $Al(OH)_3$, diaspore γ-AlOOH and diaspore α-AlOOH (Mamedov et al., 2022) according to the structure of the alumina phase. The bauxite properties vary in deposits from region to region (Bhukte et al., 2023). For example, in China, the bauxite is mainly the diaspore type; the gibbsite type is less common, accounting for only 1.54% of the total. Nevertheless, high-quality bauxite resources have been exhausted with rapid development of the aluminum industry. Fig. 1 shows world aluminum production in 2022 and China's annual aluminum production in the past 10 years. The annual output has exceeded 40 million tons (Li et al., 2022), but the bauxite reserves are only 1 billion tons, 560 million tons of which is high-sulfur bauxite, which has been gradually used in industry (Zhao et al., 2021; Zhou et al., 2018). The methods used for desulfurization of high-sulfur bauxite were wet desulfurization, calcination desulfurization, flotation desulfurization, microbial desulfurization and so on (Wu et al., 2020; Zhao et al., 2021) , and flotation has been widely applied because of its low cost and simple operation.
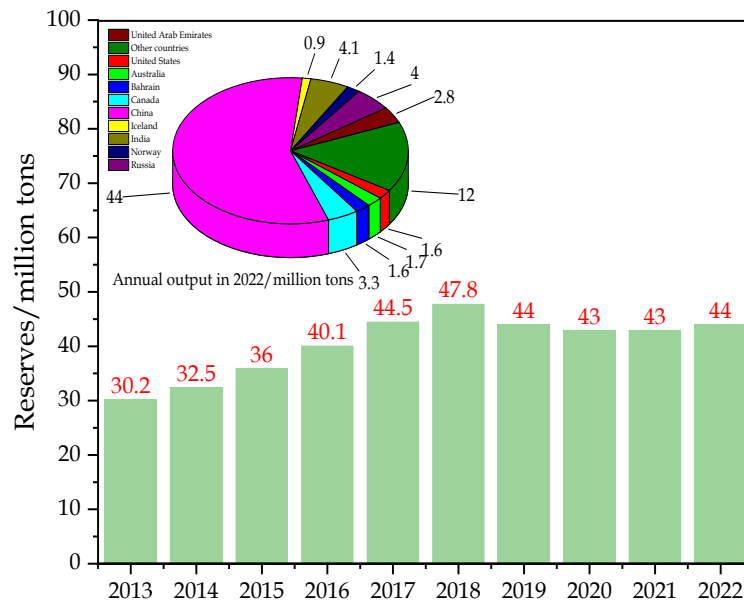
Fig. 1. The world's aluminum production in 2022 (pie chart) and China's aluminum production in the past 10 years (bar chart). (The data come from the U.S. Geological Survey)

Flotation is a method to separate target minerals from gangue minerals by different effects of minerals on liquid and gas in pulp according to the differences in physical and chemical properties of mineral particles (Cho et al., 2022; Jin et al., 2023; Sajjad and Otsuki, 2022; Saneie et al., 2022), which is one of the most effective mineral processing methods for separating and enriching target minerals (Cook and Gibson 2023; Shao et al., 2023; Xiao et al., 2022), especially for high- sulfur bauxite (Cheng et al., 2023). The main sulfide mineral in bauxite is pyrite with strong hydrophobicity, for which the most effective separation method is reverse flotation. The agent and flotation conditions are very important to obtain well mineral processing effect in the process of high- sulfur bauxite flotation (Chen and Zhang, 2022; Cheng et al., 2023). Zhou et al., (Zhou et al., 2022) synthesized quaternary ammonium ionic liquids using tetradecyl dimethyl benzyl ammonium chloride and sodium isobutyl xanthate as raw materials, which was used as flotation collector in reverse flotation of silicate and sulfur in diasporic high sulfur and high silicon bauxite. Sun et al., (Sun et al., 2021) introduced a thioether group to improve the adsorption of Fe^{2+} by the hydroxamic acid to reduce the surface energy, hydrophilicity index and free energy of bubble-mineral interaction. Chang et al., (Chang et al., 2021) added an appropriate amount of hexametaphosphate to reduce the non-selective flocculation of diaspore and gangue minerals. Nevertheless, as the most used sulfide mineral collector, xanthate is widely used in desulfurization flotation of high-sulfur bauxite (Chen et al., 2013; Owusu et al., 2015). It is worth mentioning that the change of reagent system and flotation conditions would lead to different rheological behaviors of mineral particles in pulp and foam, thereby affecting the separation performance (Zhang et al., 2020).

Rheology refers to the deformation and flow property changes of ore pulp under the action of an external force (Han et al., 2022; Sullivan and Bose, 2022), which is not only related to the mineral composition but is also strongly associated with particle sizes (Shaikh et al., 2022), pulp concentration, pH value, temperature (Wang et al., 2021) and other factors, together with the unique properties of the fine particles, such as large surface areas and high solubility. Rheological measurements have been widely used to study the particle-particle interactions of oxidized minerals, sulfide minerals, clay minerals, and gangue minerals in the pulp (Weston et al., 2020). The strong correlation between pyrite flotation efficiency and pulp rheology has been noted by many researchers. For example, Basnayaka et al. (2017) found that the well-dispersed clay minerals reduced the rate of pyrite recovery and significantly changed the rheology of the pulp. Cruz et al. (2015) found that lime resulted in higher apparent viscosities, increased the amount of copper and gold entrainment and diluted the concentrate grade. Chen et al. (2020) demonstrated that montmorillonite significantly increased the pulp viscosity and substantially reduced the pyrite recovery and grade. Adjusting the rheological properties of the

pulp is an important means to optimize flotation effect, and the additives improved the fluidity of the pulp (Zhang et al., 2022). Liu et al. (2021) added coarse-grained garnet to inhibit coagulation of sulfide ore and serpentine and reduced the apparent viscosity of the pulp system to improve flotation. Kumar and Arora (2022) found that different concentrations of sodium sulfate improved the rheological properties of microfine fly ash pulp, and the apparent viscosity gradually decreased with increasing additive concentration. In addition, it was found that the change in pulp rheology affected the fluid dynamics in the flotation tank, thereby affecting the flotation subprocesses, including gas dispersion and particle-bubble attachment (Liu et al., 2022), as well as the migration of particles and mineralized bubbles in the pulp phase (Lahiru et al., 2017).

As shown by the above summary, rheology has been widely introduced into flotation separation research, and there are few reports of flotation desulfurization of high-sulfur bauxite. In this study, the pulp rheology of pyrite and diaspore with different particle sizes were investigated with microflotation tests using butyl xanthate as collector. The effect of the microfine diaspore mass fraction on the rheological properties of the pyrite flotation pulp was studied. The effect of rheological adjustment on pulp flotation was probed with different concentrations of sodium hexametaphosphate (SHMP). Zeta potential measurements, contact angle tests and DLVO theoretical calculations were carried out. The mechanism of action for different particles in the pulp after SHMP action was analysed.

2.   Materials and methods

2.1. Raw material

Pure diaspore sample was purchased from a mine in Shanxi Province, China. Pure pyrite sample was purchased from a mine in Hunan Province, China. X-ray diffraction (XRD) show that the purity of diaspore and pyrite is high from Fig. 2. The diaspore and pyrite with big particle size were manually crushed to less than 3 mm and ground by a three-head agate grinder. The 3 narrow size fractions, 200-125 µm, 125-75 µm and 75-30 µm, along with the unclassified particle size fraction of -30 µm, were sealed and stored for the following testing. The reagents used in the experiment include CuSO4 (Guangdong Chemical Reagent Engineering Technology Research and Development Center, China), SHMP and butyl xanthate (Tianjin Kemiou Chemical Reagent Company, China), HCl and NaOH (Chengdu Jinshan Chemical Reagent Company, China). Deionized water was used in all experiments to ensure the accuracy of the testing results.
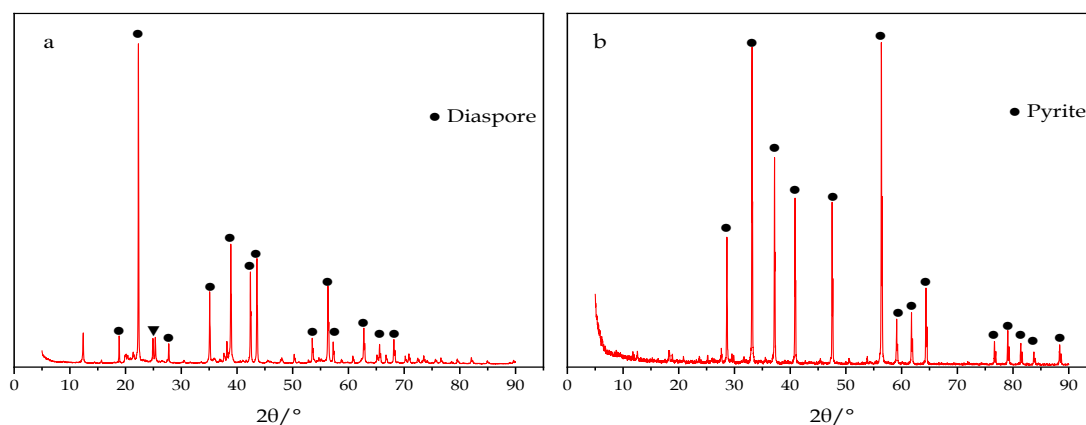

Fig. 2. XRD patterns of (a) diaspore and (b) pyrite

2.2.   Experimental methods

2.2.1. Rheological test

A rotary rheometer (ARES-G2, TA Instruments, American) was used to measure the apparent viscosity and yield stress of the pulp, as shown in Fig. 3. The gap between the inner cylinder (diameter = 32 mm) and the outer cylinder (diameter = 34 mm) was 1 mm, which was very small compared with the cup (< 3%). Therefore, the error due to the nonuniform shear generated in this small gap was negligible. The

pure minerals were stirred thoroughly after dosing according to the flotation conditions, and the pulp concentration was fixed at 20%. The pulp was stirred for 5 min it was prepared, and 20 cm^3 of the pulp was extracted and placed in a cylinder. The rotor was completely immersed in the pulp. All tests were performed at room temperature (25°C). Shear rates of 0-250 s^{-1} were selected for the point tests, according to the order of magnitude.
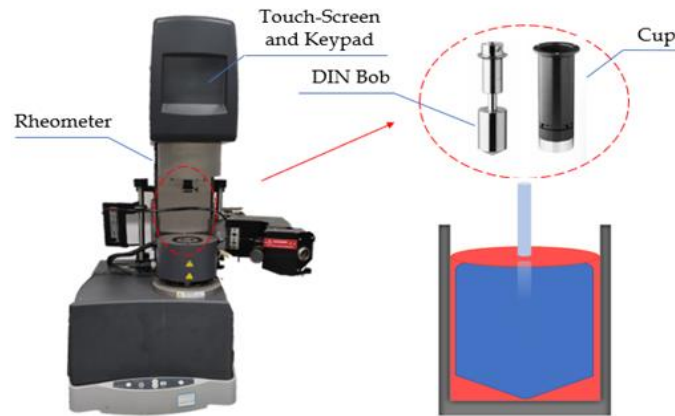

Fig. 3. Rheological test experimental device

2.2.2. Flotation test

To explore the influence of rheology on flotation, such as the S recovery rate and S grade, a 40 cm^3 flotation cell (XFGC-5~35 g, Exploration Machinery Plant, Jilin Province, China) was used for testing, and the impeller speed was 1992 rpm. The detailed preparation process was as follows: pyrite of mass fraction and 32 cm^3 of deionized water were added into a beaker for ultrasonic washing for 5 min (Cao et al., 2017); pyrite and diaspore were added to the flotation cell in turn and allowed to rise to a fixed position; the main shaft mixer was opened and fully stirred for 2 min, and the pH was maintained at 8-9 with NaOH or HCl; CuSO$_4$ was added at the beginning of the second stirring for 2 min, and then butyl xanthate was added and stirred for 3 min; finally, the terpenic oil was added and stirred for 1 min, and the flotation time was 4 min at room temperature. The time for each stirring stage was controlled to within ±1 s in the above process. The resulting foam products were filtered and dried at low temperature to calculate the recovery rate and test the sulfur content. The flotation reagent system is shown in Table 1. The experimental apparatus for microflotation is shown in Fig. 4.

Table 1. List of main reagents

Reagent	Amount	Purity
HCl	1%	Analytically pure
NaOH	1%	Analytically pure
SHMP	0.05 mg/kg, 0.50 mg/kg	Analytically pure
CuSO$_4$	0.10 g/kg	Analytically pure
C$_4$H$_9$OCSSNa	0.30 g/kg	Analytically pure
C$_{10}$H$_{18}$O	0.15 g/kg	Technical pure

2.2.3. Dynamic potential tests of the mineral surfaces

Particle analyzer (Delsa Nano C, Beckman Coulter Company, American) was used to determine the electrokinetic potential of the mineral surface. Diaspore and pyrite were ground to -30 μm using a three-headed agate grinder. A total of 40 mg of sample was weighed and converted into pulp with a mass concentration of 0.1%. The mineral particles were fully dispersed by stirring evenly after ultrasonic treatment for 2 min. The pH 8-9 of the pulp was adjusted to 8-9, the desired concentration of the collector butyl xanthate and SHMP were added, and the pulp was stirred for 5 min to allow the mineral and reagent to interact sufficiently. An appropriate amount of supernatant was extracted and injected into

the spot pool of the point tester to test the zeta potential of the mineral surfaces before and after treatment with SHMP and different pH. Each condition was tested 3 times, and the average value was used as the final result.
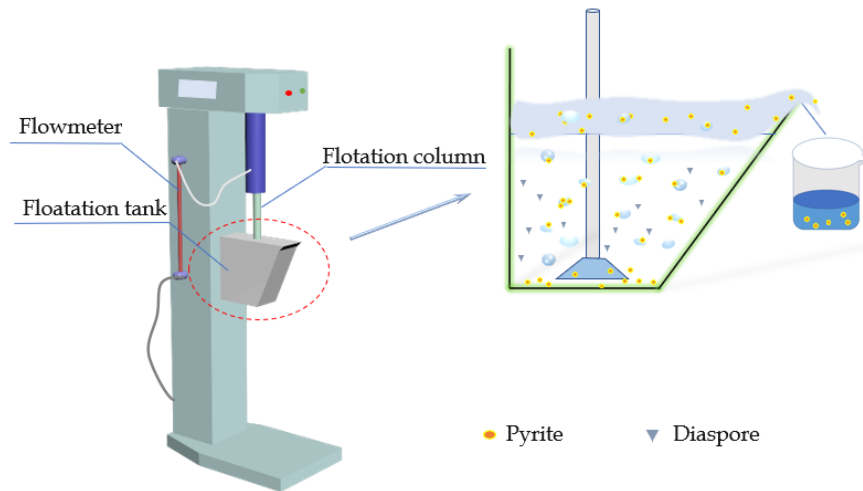

Fig. 4. Schematic diagram of the foam flotation experimental device

2.2.4. Contact angle tests

A contact angle instrument (HKCA-PV35, Beijing HaKe Test Instrument Factory, China) was used to determine the electrokinetic potential of the mineral surface. Pyrite particles with sizes of approximately 1 cm and complete structures were selected from the sample. The surfaces of the pyrite particles were polished with 600-, 2000- and 6000-mesh emery cloths to make the pyrite clear, and the polished surface was used for contact angle testing. The pyrite was then treated in 3 different ways: (1) by immersion in a 1% butyl xanthate for 20 min; (2) further immersion in a 0.05 mg/kg SHMP solution for 20 min, after soaking in 1% butyl xanthate solution for 20 min; and (3) further immersion in a 0.50 mg/kg SHMP solution for 20 min, after soaking in 1% butyl xanthate solution for 20 min.

2.2.5. Sulfur content tests

A microcomputer Coulomb sulfur meter (CLS-3000, Jiangsu Guochuang Analytical Instrument Company, China) was used to analyse the total sulfur contents of the samples. The product of the flotation concentrate prepared as in Section 2.2.2 was weighed at low temperature and then used to test the S (sulfur) content. The sample mass was 50 mg and was evenly tiled in the combustion boat and covered with tungsten trioxide. The combustion temperature was 1050℃.

3. Results and discussion

3.1. Rheology

3.1.1. Effect of particle sizes on pulp rheology

The shear rates and shear stresses of the diaspore pulp and pyrite pulp with different particle sizes were measured to explore the influence of particle size on the rheology, and the fluid properties of the pulp system were determined by fitting the shear rate-shear stress curve. Fig. 5(a) shows that diaspore pulp with a mass fraction of 20% and particle sizes of 75-125 μm, 45-75 μm, and 30-45 μm behaved as Newtonian fluids with a linear shear stress versus shear rate curve being passing through the origin (Zhang and Peng 2015). The addition of a 20% mass fraction of -30 μm diaspore, however, caused the pulp to become as a non-Newtonian fluid with yield stress, and the increased rate of shear stress gradually decreased and became stable with increasing of shear rate. It is worth noting that as the shear rate continued to increase, the shear stress of the pulp increased approximately linearly, which was basically consistent with the Bingham rheological model (Fu et al., 2022), and the yield stress of the fluid fluctuated with changes in the external force (Zhang et al., 2023). Furthermore, the effect of fine diaspore

on the rheology of the pulp was more obvious than that of coarse diaspore because of the increase in shear stress of the diaspore with decreases in particle size at the same shear rate. As shown in Fig. 5(b), the shear stress-shears rate curves for the pyrite pulps with all particle sizes showed little difference and were basically linear curves, indicating Newtonian fluids. Diaspore and pyrite had different effects on the rheological properties of the pulp, and the different rheological properties of the diaspore pulp and pyrite pulp systems at the same mass fraction might be related to the electrochemical properties and particle properties of the different mineral particles.
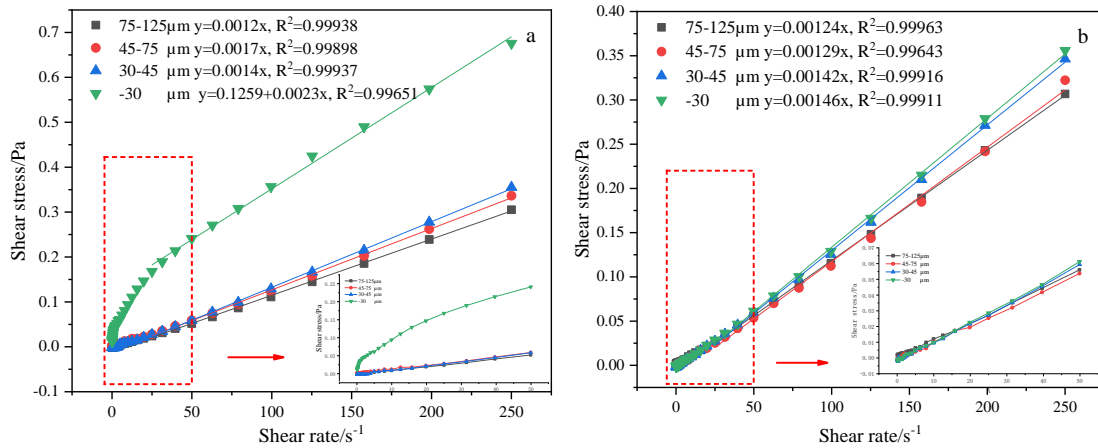

Fig. 5. Shear rate-shear stress curves of pulp with different particle sizes; (a) diaspore and (b) pyrite

3.1.2. Effect of mass fraction on the rheology

The rheological properties of the pulp system were changed significantly by changes in the mineral properties, which affected the flotation pulp environment. Diaspore was easier to mud than pyrite, which affected the separation of pyrite in the grinding process. The shear rate-shear stress curves for different mass fractions of pyrite monohydrate were measured, and the experimental results are shown in Fig. 6. The particle sizes of diaspore and pyrite used in the experiment were -30 µm. The shear rate-shear stress curve gradually moved up, and the shear stress changed significantly as the mass fraction of the diaspore was increased. Diaspore increased the viscosity for the pulp, resulting in a certain yield stress of the diaspore-pyrite mixed pulp (mixed pulp) because the fine-grained diaspore pulp was well dispersed and may have formed a uniform network structure. The mixed pulp had an initial yield stress at low shear rates, and the small aggregates formed in the pulp suspension decompose with increasing shear rate. The yield stress indicated that a complex structure was formed in the mixed pulp suspension. Therefore, the rheology of the pulp system deteriorated and collisions between the pyrite and bubbles influenced (Weston et al., 2020).
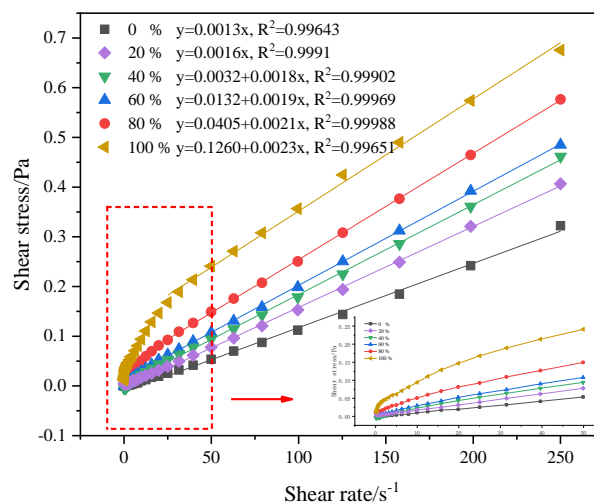

Fig. 6. Effect of diaspore mass fraction on the shear rate-shear stress curves of mixed pulp

3.1.3. Rheology regulation of diaspore-pyrite pulp

The rheology of flotation pulp is an important factor affecting mineral flotation. The flow of mineralized bubbles from the bottom of the pulp to the surface of the pulp did not lead to mineralization of the flotation bubbles at high pulp viscosities. SHMP is used as for its good pulp regulation capability in the field of mineral flotation. The apparent viscosity and yield stress of the pulp were reduced, and dispersion of the particles was enhanced by the added SHMP (Zhang et al., 2022). Therefore, SHMP was used to regulate the rheology of the mixed pulp in this study. The shear rate-shear stress curves for -30 µm mixed pulp with two concentrations of SHMP were measured, and the test results are shown in Fig. 7. According to the pulp shear rate-shear stress curve, the mass fraction of diaspore in the presence of 0.05 mg/kg SHMP were 40%, 60% and 80%, which conformed to the Bingham fluid model. The same conclusion was obtained when the mass fraction of diaspore was 60% and 80% with 0.50 mg/kg SHMP. Fig. 7 shows that the shear rate-shear stress curve moved up with increases in the mass fraction of diaspore, but the amplitude of the upwards movement was obviously reduced, especially when the amount of added SHMP was 0.50 mg/kg. In addition, the distribution of the shear rate-shear stress curve for the mixed pulp was more concentrated than that seen with 0.05 mg/kg when the amount of SHMP added was 0.50 mg/kg. Therefore, the addition of 0.50 mg/kg SHMP was more effective than the addition of 0.05 mg/kg SHMP.
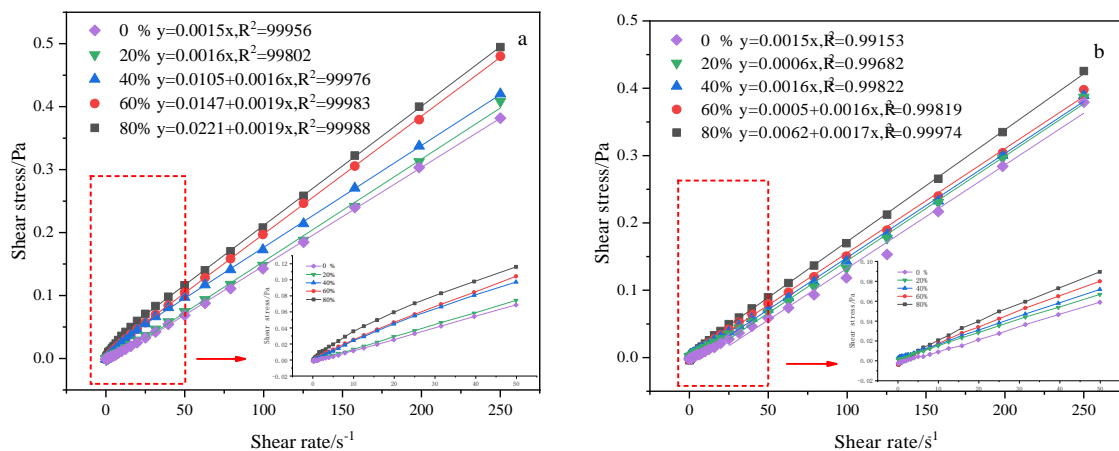

Fig. 7. Shear rate-shear stress curve for mixed pulp in diaspore mass fraction with SHMP concentration of (a) 0.05 mg/kg and (b) 0.50 mg/kg

3.2. Effect of the rheological properties of mixed pulp on flotation separation of pyrite

3.2.1. Effect of pyrite particle size on pulp viscosity and flotation recovery

The apparent viscosity of the pulp is one of the main parameters used to evaluate the rheological properties of flotation pulp (Farrokhpay 2012). The apparent viscosity and yield stress of the pulp in the shear rate range 25-250 s^{-1} were obtained by Bingham fitting of the shear rate-shear stress curve for the pulp. With a pulp concentration of 20%, the apparent viscosities of the diaspore pulp and pyrite pulp with different particle sizes are shown in Fig. 8. For both diaspore pulp and pyrite pulp, the apparent viscosity of the pulp increased gradually with decreasing particle size, especially the apparent viscosity of the diaspore pulp, which increased obviously. The apparent viscosity of the diaspore pulp with particle sizes of -30 µm was 89.80% higher than that of pyrite pulp with the same particle sizes. Diaspore pulp with particle sizes of -30 µm was the main factor leading to viscosity enhancement in the mixed pulp. Taking the flotation recovery of pyrite with different particle sizes as an example, the effect of the pulp apparent viscosity on the flotation separation of pyrite was determined, as shown in Fig. 8. The apparent viscosity of the pulp increased gradually with decreasing mineral particle sizes, while the recovery rate for pyrite first increased and then decreased. The intermediate grade showed better performance in the flotation process (Yang et al., 2019). The apparent viscosity of the pulp did not seem to have a correlation with the recovery rate, but some researchers have shown that slight increase in the viscosity of the pulp increase the stability of the bubble particles and enhanced flotation separation.

Whether the pyrite pulp should also lead to a similar conclusion needs further study. The recovery rates for pyrite with grain sizes of 45-75 μm were up to 58.00%, which were much higher than those of pyrite with grain sizes of 30-45 μm and -30 μm. Pyrite adhesion on the bubble surfaces was not stable during the flotation process, and it easily fell off with increasing particle sizes, resulting in a decrease in flotation recovery. The rheological properties of pyrite pulp with different particle sizes change little, and the flotation recovery rate of the pyrite first increased and then decreasing with particle sizes, indicating that the flotation recovery rate of pyrite with closely related to the particle sizes.
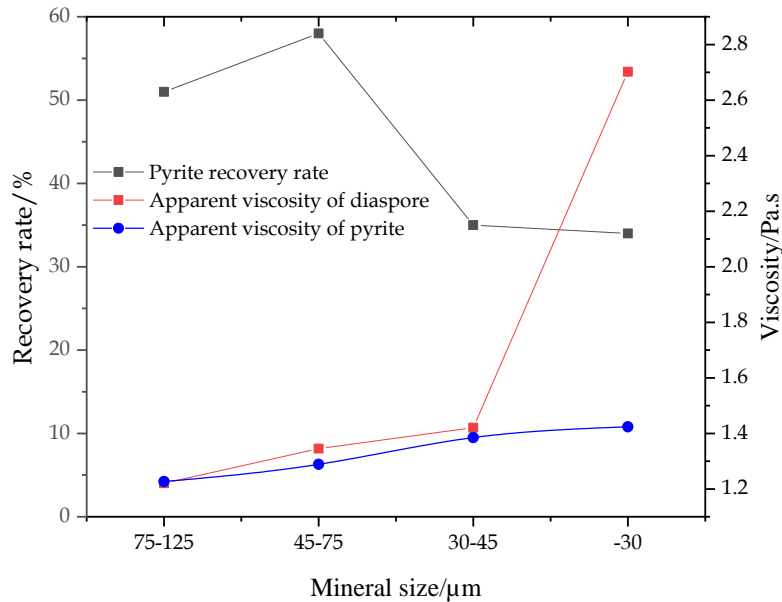

Fig. 8. Recovery rates or pyrite with different particle sizes and the apparent viscosities of diaspore and pyrite pulps with different particle sizes

3.2.2. Effect of apparent pulp viscosity on flotation separation of pyrite

The rheological curve for the pulp in the shear rate range of 25-250 s^{-1} was obtained by fitting the pulp shear rate-shear stress curve. The flotation of pyrite different mass fractions of diaspore was studied. The apparent viscosity and yield stress of the non-Newtonian pulp fluid were calculated by fitting the shear rate-shear stress curve for the pulp. The apparent viscosity curves for pyrite pulp with different mass fractions of diaspore at a yield stress and shear rate of 100 s^{-1} are shown in Fig. 9. The apparent viscosity of the pulp was increased by 19.38% with a 20% mass fraction of diaspore, the S recovery rate of the S concentrate was increased by 8.89% to the maximum value, and the S concentrate grade was 33.44%. The S recovery rate and grade of the S concentrate decreased gradually with increasing diaspore mass fraction. The increased rate of S recovery from the S concentrate may have resulted from the addition of diaspore, which increased the apparent viscosity and yield stress of the pulp and increased the probability of interaction between the pyrite and bubbles. Mineral entrainment was more obvious with increased viscosity, which caused the flotation recovery rate to increase slightly (Wang and Liu 2021).

The pulp was still a Newtonian fluid, and the yield stress were not measured when the mass fraction of diaspore was 0%-20%. The pulp gradually transformed into a non-Newtonian fluid, and the yield stress of the pulp system increased gradually to 0.0405 Pa with continuous increases in the diaspore mass fraction. It was expected that the high concentration of pulp would change from a Newtonian fluid to a non-Newtonian fluid. With mass fractions of 40% and 60%, the yield stress of the pulp increased. The S concentrate recovery rate from the pulp decreased to 32.99%, the S concentrate grade was 7.78% when the mass fraction of diaspore gradually increased to 80%, and the apparent viscosity and yield stress were 0.00252 Pa·s and 0.0405 Pa·s, respectively. The fine diaspore exhibited good dispersibility and hydrophilicity in water, and the resulting network structure increased downwards adhesion of the bubbles during the rise process, so that the fine-grained mineral coating on the mineral

surface prevented the collector from adsorbing on the surfaces of the useful minerals (Chen et al., 2019); this reduced the salinity of the bubbles and affecting the flotation of pyrite (Bournival et al., 2016). In conclusion, the effects of the hydrodynamic interactions were dominant with low concentrations of diaspore. The friction interaction and apparent viscosity between particles per unit volume increased sharply with increasing pulp concentration. The flotation recovery rate of pyrite first increased and then decreased, and the grade decreased gradually. Therefore, the change in pulp rheology had a significant effect on the recovery rate of pyrite.
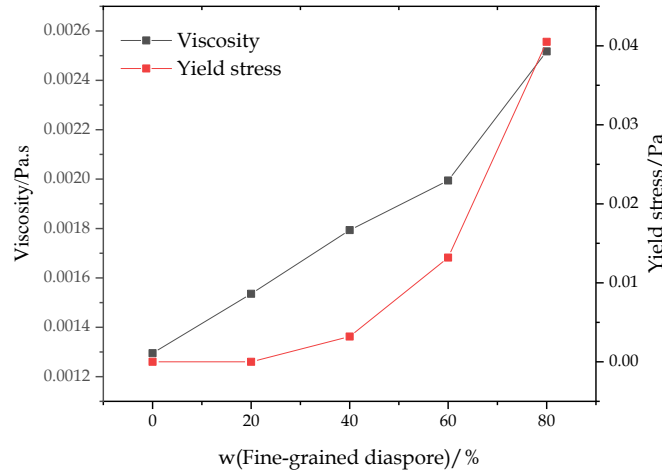

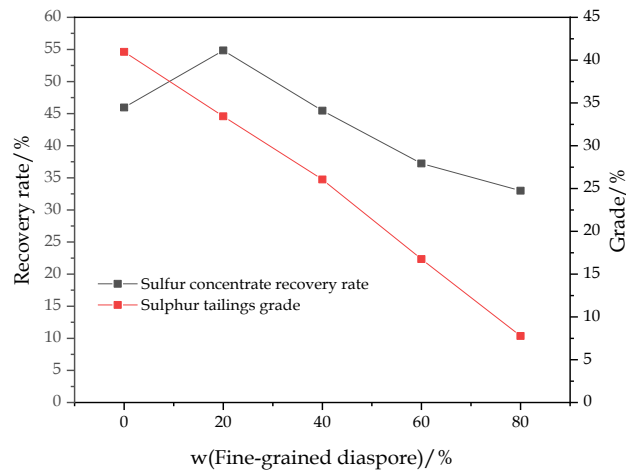Fig. 9. Effect of different diaspore mass fractions on the apparent viscosity and yield stress

Fig. 10. Effect of the diaspore mass fraction on pyrite (a) recovery rate and (b) grade

3.2.3. Effect of rheology regulation on apparent viscosity

The SHMP hydrolysis products $[H_2PO_4]^-$ and $[HPO_4]^{2-}$ were the active components of the dispersed minerals, which reacted with a variety of metal ions and change the hydrophilicity of the mineral surface (Zhou et al., 2023). The above results also showed that the addition of SHMP regulated the rheology of the mixed pulp. In this study, SHMP was used to adjust the rheology of the mixed pulp. The apparent viscosity and yield stress curves for the mixed pulp with SHMP are shown in Fig. 11. The apparent viscosity and yield stress of the mixed pulp decreased with increasing of SHMP dosage. Fig. 11(a) shows that the viscosity of the mixed pulp decreased slightly by 3.01% when 0.05 mg/kg SHMP was added to give a mass fraction of 60%, but the apparent viscosity decreased by 17.06% when the mass fraction was 80%. The viscosity of the mixed pulp with 0.50 mg/kg SHMP was lower than that seen with the addition of 0.05 mg/kg SHMP. For example, the viscosity of the pulp with 0.50 mg/kg SHMP was 32.14% lower than that without SHMP when the mass fraction of diaspore was 80%. Fig. 11(b) shows that when the mass fraction of diaspore was 60%, 0.05 mg/kg and 0.50 mg/kg SHMP reduced the yield stress of diaspore pyrite pulp by 34.85% and 96.21%, respectively. These results

showed that the addition of SHMP reduce the energy barrier to fluid movement of the pulp and thus reduced the yield stress.

As shown in Fig. 12(a), with the two SHMP concentrations, the S recovery rates of the S concentrate from the mixed pulp were improved. The effect of SHMP on the flotation recovery rate was most obvious when the content of diaspore was 60%. The apparent viscosity of with 0.50 mg/kg SHMP was 21.76% lower than it was with the addition of 0.05 mg/kg SHMP, but the S recovery rate of the S concentrate was also reduced by 14.94%. Therefore, SHMP improved the recovery rate of pyrite. It is preliminarily thought that the increased S recovery rate from the S concentrate with added SHMP was related to the decreased pulp rheology. Fig.12(b) shows that mineral entrainment was more obvious in the flotation process (Hu and Shi 2022), and the S grade in the S concentrate decreased gradually with increasing diaspore mass fraction. It is worth noting that the S grade in the S concentrate first increased and then decreased with increasing SHMP concentration and the same mass fraction of diaspore. These above results showed that SHMP regulated the rheology of the mixed pulp and facilitated flotation separation of the diaspore and pyrite, but an excessive amount of SHMP inhibited pyrite flotation.
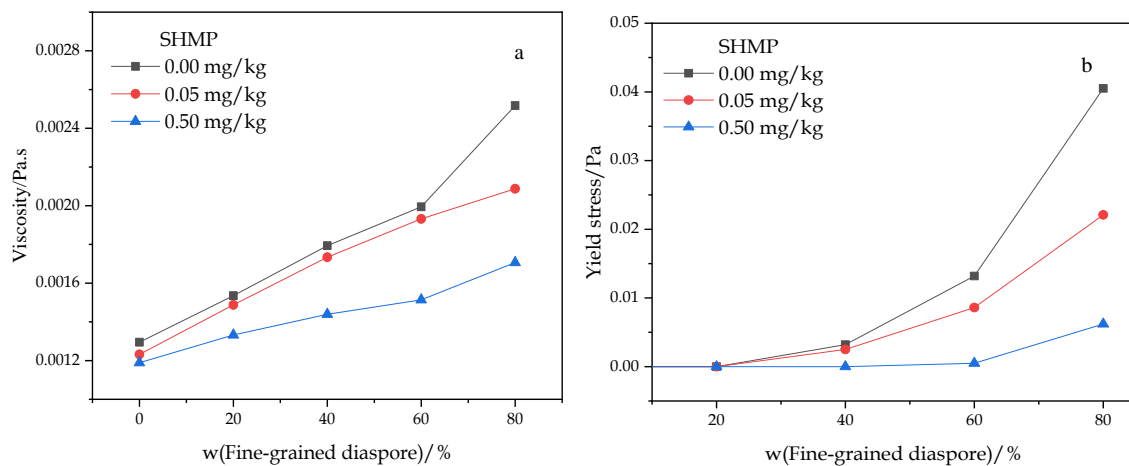

Fig. 11. Effect of SHMP on (a) the apparent viscosity and (b) the yield stress of the mixed pulp in different diaspore mass fractions
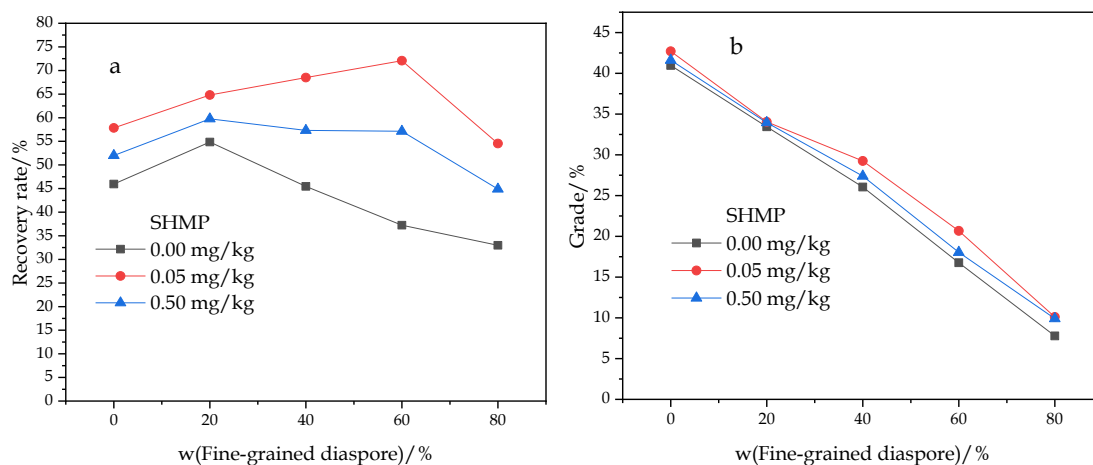

Fig. 12. Flotation effect of diaspore with different mass fractions on pyrite in the presence of SHMP; (a) S concentrate recovery rate and (b) S tailings grade

3.3. Interactions between pyrite and diaspore

The interactions between fine-grained pyrite and diaspore in the flotation pulp were studied to reveal the influence of the rheology on flotation of fine-grained pyrite because the mechanisms for aggregation and dispersion of mineral particles in the pulp fluid were explained with the DLVO theory. The classical DLVO theory holds that the interaction forces between particles in a suspension depend on van der

Waals attraction and electrostatic repulsion of the electric double layer, and this is expressed as in Formula (1):

$$V_{DT} = V_{WA} + V_{ER} + V_{HA} \tag{1}$$

where V_{DT} is the sum of the interaction forces between particles; V_{WA} is the van der Waals interaction force; V_{ER} is the electrostatic force of the electric double layer; and V_{HA} is hydrophobic interaction attraction. In the flotation system, there were many other forces between the hydrophilic or hydrophobic particles due to the presence of flotation reagents, including the hydration interaction repulsion energy, hydrophobic interaction attraction energy, and space stabilization energy. Pyrite is hydrophobic in the pulp system with the collector butyl xanthate, and calculations of the interaction forces between particles should also consider the hydrophobic interactions between pyrites particles.

3.3.1. Van der Waals force between particles

The average particle sizes of the -30 μm microfine diaspore and pyrite were 15 μm. The van der Waals interaction between mineral particles was considered to be the force between two spheres with radii of R1 and R2 (Bai et al., 2020). This is expressed in Formula (2) (Wang et al., 2022).

$$V_{WA} = \frac{-A}{6H} \times \frac{R_1 R_2}{R_1 + R_2} \tag{2}$$

where A is the effective Hamaker constant between particles in the medium, J; R_1 and R_2 are the radii of two different mineral particles, nm; and h is the distance between the mineral particles, nm. The effective Hamaker constant A_{213} for different particles 2 and 3 in medium 1 is expressed as in Formula (3) (Chen et al., 2021; Zhanglei et al., 2020).

$$A_{213} = A_{11} + A_{23} - A_{12} - A_{13} = \sqrt{A_{11} - A_{22}}\sqrt{A_{11} - A_{33}} \tag{3}$$

where A_{11}, A_{22} and A_{33} are the Hamaker constants for butyl xanthate, pyrite and diaspore in a vacuum, which are $A_{11} = 5.0 \times 10^{-20}$, $A_{22} = 12 \times 10^{-20}$ and $A_{33} = 15.2 \times 10^{-20}$. Then, $A_{213} = 8.5 \times 10^{-20}$ was calculated with Formula (3). The mineral particles were approximated as spheres with radii of R. Fig. 13 shows that the van der Waals forces were always attractive, so the van der Waals forces dominated aggregation of the microfine diaspore and pyrite, and the attraction gradually decreased with increasing distance between the particles. The gravitational force between the particles gradually disappeared and the particles were completely dissociated when the particle spacing H > 38 nm.
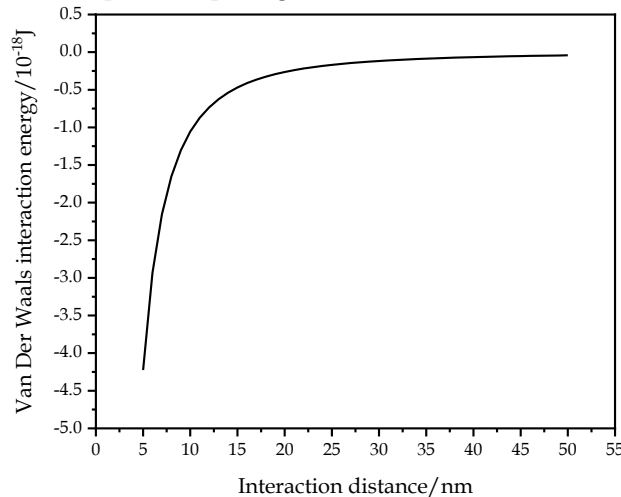

Fig. 13. van der Waals interaction energy

3.3.2. Electrostatic repulsion between particles

The electrostatic force V_{ER} between two mineral particles can be calculated with Formula (4) (Chen et al., 2021; Fu et al., 2021; Zhang et al., 2021).

$$V_{ER} = \frac{\pi \varepsilon R1 R2}{R1 + R2}(\varphi_1^2 + \varphi_2^2)\left[\frac{\varphi 1 \varphi 2}{\varphi_1^2 + \varphi_2^2} p + q\right] \tag{4}$$

$$p = ln\left[\frac{1+exp(-kH)}{1-exp(-kH)}\right] \tag{5}$$

$$q = ln[1 - exp(-2kH)] \tag{6}$$

where ε is the absolute dielectric constant of the medium, C²/(J.nm), the calculation method is : $\varepsilon = \varepsilon_r \times \varepsilon_0$, ε_r is the relative dielectric constant of the dispersion medium, taking the relative dielectric constant of butyl xanthate $\varepsilon_r = 78.5$, ε_0 is the absolute dielectric constant in vacuum $\varepsilon_0 = 8.854 \times 10^{-12}$, and $\varepsilon = 6.95 \times 10^{-10}$ in butyl xanthate solution (Hu and Liang 2020); φ_1 and φ_2 are the surface potentials of the two mineral particles (which can be replaced by the zeta potential), mV; and k is the Debye length, that is, the thickness of the electric double layer on the particle surface, nm. The calculation method is: $k^{-1} = 0.304/c^{1/2}$, c is the concentration of the collector butyl xanthate solution, mol/L, and the reciprocal of the Debye length is taken as $k_1 = 0.1274$ nm^{-1}. As shown in Table 2, the surface potential of pyrite decreased with increasing SHMP concentration at pH 8-9. Electrostatic attraction was also considered one of the mechanisms for the interaction between the collector and pyrite (Cheng et al., 2023). The electrostatic energy curve for the particles in the pulp gradually moved to the right with increasing SHMP concentration as shown Fig. 14. The electrostatic force between the particles increased gradually due to the addition of SHMP when the distance between the particles was held constant, which enabled full dispersion of the particles. The electrostatic force was always the only repulsive force between the diaspore and pyrite, and was the main driving force for adsorption of the cationic molecular fragments on the surfaces of the particles.

Table 2. Zeta potential of pyrite and diaspore in butyl xanthate system.

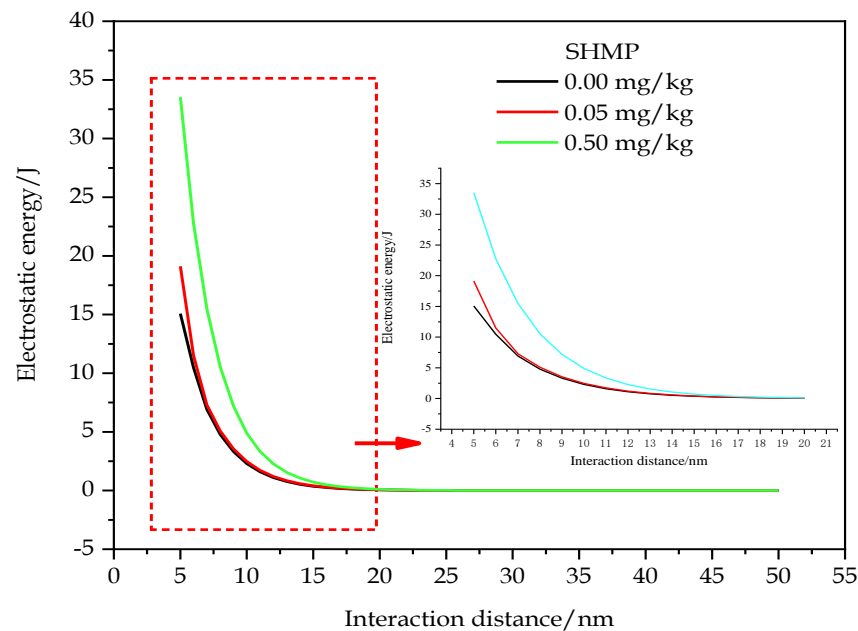| SHMP/mg/kg	Surface potential of pyrite /mV	Surface potential of diaspore /mV
0.00	-26.29	-44.61
0.05	-31.77	-50.26
0.50	-41.80	-44.49

Fig. 14. Electrostatic interaction energy

3.3.3. Hydrophobic force between particles

The hydrophobic interaction energy (V_{HA}) between identical particles as a function of the contact angle is expressed as in Formulas 7, 8 and 9 (Cheng et al., 2020).

$$V_{HA} = -2.51 \times 10^{-3} R k_1 h_0 \, exp\left(-\frac{H}{h_0}\right) \tag{7}$$

$$k_1 = \frac{exp(\frac{\theta}{100}-1)}{e-1} \tag{8}$$

$$h_0 = (12.2 \pm 1.0)k_1 \tag{9}$$

where θ is the contact angle of the mineral particles, °; k_1 is the incomplete hydrophobic coefficient; h_0 is the decay length, nm. Most evidence supports the operation of hydrophobic forces between hydrophobic surfaces, but the origin of the hydrophobic forces is still controversial. Therefore, Formula 7 is an empirical expression, which is derived from the attenuation index. The surface hydrophobicity was increased gradually by the addition of SHMP, as shown by the contact angle data for pyrite in Table 3. Fig. 15 shows the hydrophobic interaction energy of pyrite. The added of dispersant increased the hydrophobicity of the pyrite, which facilitated the adsorption of pyrite and bubbles.

Table 3. Contact angle of deionized water on pyrite surface

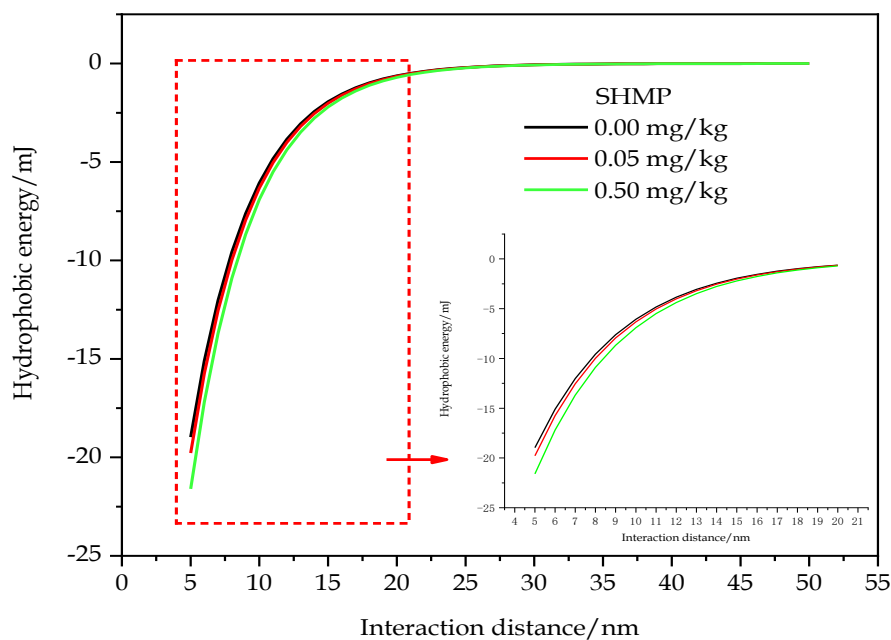| SHMP/mg/kg	Water contact angle/°
0.00	51.80
0.05	53.90
0.50	58.30

Fig. 15. Hydrophobic interaction energy

The effect of the SHMP concentration on the interaction energy between particles with mixed pulp in the butyl xanthate was calculated and analysed, as shown in Fig. 16. The total potential energy for the interactions between particles in the pulp was determined. The particles always showed strong repulsive forces at distances of 5-20 nm. The repulsive force increased gradually with the increasing of SHMP concentration for distances of 5-20 nm. The experimental results showed that the electronegativity between the microfine pyrite and diaspore in the butyl xanthate system was increased by adding SHMP. The electrostatic force of the electric double layer between the particles was enhanced, the repulsion between the particles in the pulp was increased, and the degree of particle dispersion in the system was improved.

3.4. Mechanism for rheological regulation of flotation in a diaspore-pyrite mixed pulp

The rheology of the pulp was regulated, flotation separation of the diaspore and pyrite was enhanced, the collisions between pyrite particles and bubbles were improved, the capacity for adsorption of pyrite particles on the bubbles were enhanced, and the flotation separation of diaspore and pyrite was

promoted by adding reagents to regulate the rheology of the pulp. The specific mechanism is shown in Fig. 17 and Fig. 18. The surface energy was high, and the adsorption capacity was strong, which resulted in the formation of mineral aggregates due to the presence of fine diaspore in the mixed pulp. The complex rheology of the pulp inhibited the action of pyrite and the collector and the adsorption of pyrite on the bubbles. In particular, the rheology of the pulp was more complicated, and this was more obvious when the content of the microfine diaspore was very high. The rheology of the pulp was regulated by adding different concentrations of SHMP. SHMP acted on the mineral surface in the mixed pulp, which increased the electronegativity of the mineral surfaces, enhanced the interactions between mineral particles, dissociated the aggregated particles, reduced the apparent viscosity and yield stress of the mixed pulp, enabled collisions between the pyrite particles and bubbles and adsorption of the pyrite particles on the bubbles, and reduced the resistance of the ore-bearing bubbles to floatation. Additionally, it reduced the coverage of diaspore on the surface of the pyrite, promoted the action of butyl xanthate on the surface of pyrite, and adhered to the bubbles more effectively during bubble flotation, thus improving the flotation recovery rate of pyrite.
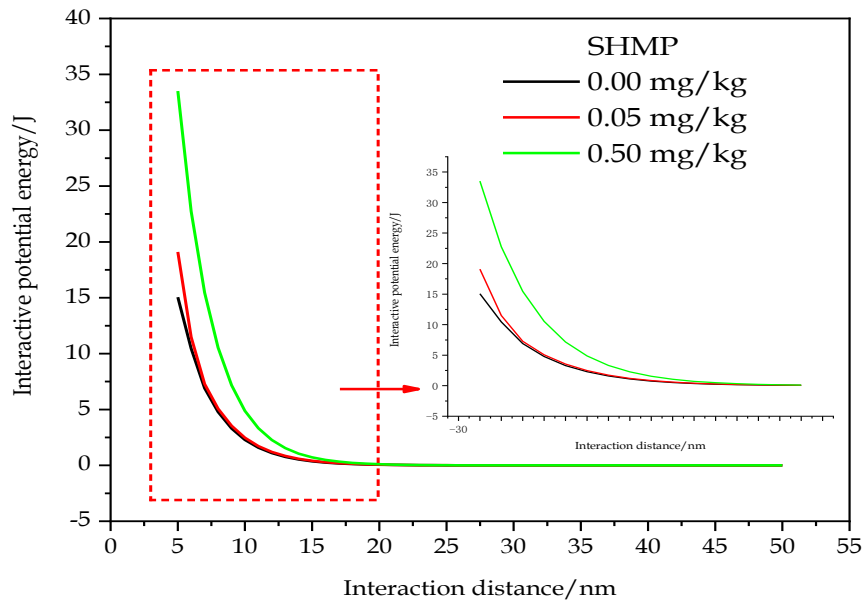

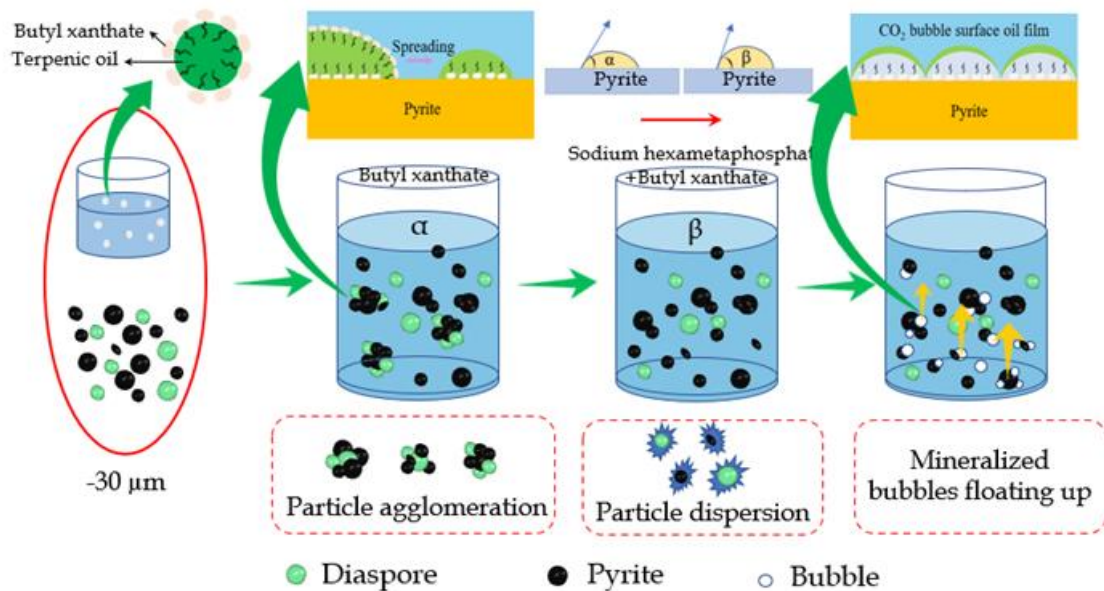Fig. 16. Total potential energy for interaction between particles

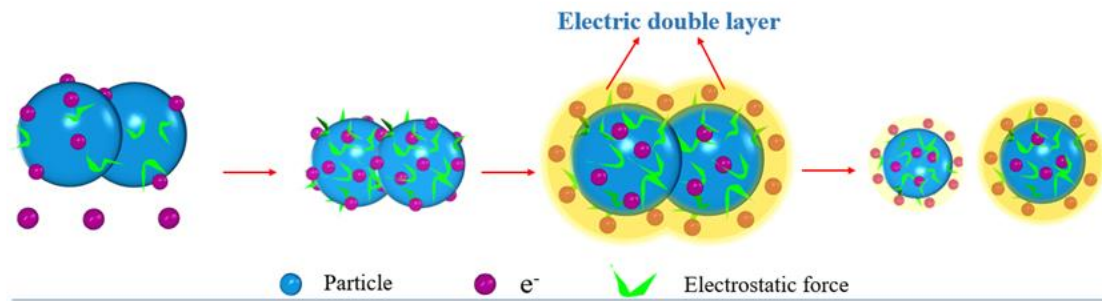Fig. 17. Mechanism of SHMP on mineral flotation

Fig. 18. Action diagram of SHMP

4. Conclusions

(1) The diaspore pulp with mass concentration of 20% and particle sizes of 75-125 µm, 45-75 µm and 30-45 µm were Newtonian fluids. The pulp was a non-Newtonian fluid with yield stress when the mass fraction of the -30 µm diaspore was 20%. However, the shear stress-shear rate curves for the pyrite pulp with a mass fraction of 20% and particle sizes of 75-125 µm, 45-75 µm, 30-45 µm and -30 µm were basically linear, indicating Newtonian fluids. The content of the fine diaspore was an important factor affecting the apparent viscosity and yield stress of the mixed pulp.

(2) The apparent viscosity and yield stress of the pulp increased gradually as the mass fraction of diaspore in the mixed pulp was increased, which reduced the turbulence intensity in the pulp to a certain extent and improved the stability of the bubbles. The apparent viscosity of the pulp was increased by 19.38%, the S recovery rate from the S concentrate was increased by 8.89% when the mass fraction of pulp was 20%, and the maximum value was reached. The S grade of the flotation S concentrate was 33.44%. Mineral entrainment obviously reduced the S recovery rate from the S concentrate and the S grade in the flotation concentrate with a further increase in the diaspore mass fraction. With further increases in the mass fraction of diaspore, higher surface energies and stronger adsorption led to aggregation between minerals, which hindered the functions of the pyrite and the collector and the adsorption of pyrite on the bubbles, while increasing the resistance to floatation of the ore bubbles, coupled with obvious mineral entailing, resulting reduced of S recovery and lower S grades in the flotation concentrate.

(3) SHMP acted on the mineral surfaces in the mixed pulp, which increased the electronegativity of the mineral surfaces, enhanced the interactions between mineral particles, dissociated the aggregated particles, reduced the apparent viscosity and yield stress of the mixed pulp, which decreased with increasing SHMP dosage. This enabled the collisions between the pyrite particles and bubbles and the adsorption of pyrite on the bubbles, and reduced the resistance to flotation of the ore-bearing bubbles. The amount of SHMP added was 0.05 mg/kg when the diaspore mass fraction was 60%, the apparent viscosity of the pulp was reduced by 3.01%, and the S recovery rate from the S concentrate and S grade of the S concentrate were increased by 34.83% and 4.67%, respectively. However, excess SHMP inhibited pyrite flotation. Although the apparent viscosity of the pulp was reduced by 24.12% when the amount of SHMP added was 0.50 mg/kg, the S recovery rate and S grade of the S concentrate decreased.

Acknowledgments

References

BAI H., LIU Y., ZHAO Y., CHEN T., LI H., CHEN L., SONG S., 2020. *Regulation of coal flotation by the cations in the presence of clay*. Fuel 271, 117590.

BASNAYAKA L., SUBASINGHE N., ALBIJANIC B., 2017. *Influence of clays on the slurry rheology and flotation of a pyritic gold ore*. Appl. Clay. Sci. 136, 230-238.

BHUKTE P.G., DAWARE G.T., MASURKAR S.P., PANCHAL M.S., CHADDHA M.J., 2023. *Effect of Geological, Mineralogical Characteristics on Grindability of Bauxite: A Case Study of Indian Lateritic Bauxite Deposits*. J. Geol. Soc. India 99, 55-60.

BOURNIVAL G., ATA S., WANLESS E.J., 2016. *Behavior of Bubble Interfaces Stabilized by Particles of Different Densities.* Langmuir 32, 6226-6238.

CAO Q., CHENG J., FENG Q., WEN S., LUO B., 2017. *Surface cleaning and oxidative effects of ultrasonication on the flotation of oxidized pyrite*. Powder Technol. 311, 390-397.

CHANG Z., SUN C., KOU J., FU G., QI X., 2021. *Experimental and molecular dynamics simulation study on the effect of polyacrylamide on bauxite flotation.* Miner Eng 164, 106810.

CHEN A., ZHANG Q., 2022. *Influence of measuring process properties on phosphate rock slurry rheology based on Brookfield method.* Physicochem. Probl. Miner. Process. 58(6), 156202.

CHEN L., ZHAO Y., BAI H., AI Z., CHEN P., HU Y., SONG S., KOMARNENI S., 2020. *Role of Montmorillonite, Kaolinite, or Illite in Pyrite Flotation: Differences in Clay Behavior Based on Their Structures*. Langmuir 36, 10860-10867.

CHEN L., ZHAO Y., BAI H., WEN T., AI Z., SONG S., 2021. *Effect of protonation and deprotonation reactions of clay on regulating pyrite flotation in the presence of clay.* Colloids and Surfaces A: Physicochemical and Engineering Aspects 609, 125654.

CHEN P., CHEN Y., LIU H., LI H., CHAI X., LU X., SUN W., WANG H., LUO Y., WANG X., 2021. *Novel Approach for Fine Ilmenite Flotation Using Hydrophobized Glass Bubbles as the Buoyant Carrier.* Minerals 11, 231.

CHEN W., CHEN Y., BU X., LONG T., ZHANG G., CHEN F., LIU R., JIA K., SONG Y., 2019. *Rheological investigations on the hetero-coagulation between the fine fluorite and quartz under fluorite flotation-related* conditions. Powder Technol. 354, 423-431.

CHEN X., PENG Y., BRADSHAW D., 2013. *Effect of regrinding conditions on pyrite flotation in the presence of copper ions*. Int. J. Miner. Process. 125, 129-136.

CHEN Y., ZHANG T., LV G., CHAO X., YANG X., 2022. *Research on the Dealkalization Treatment of Bauxite Residue and Deep Extraction of Alumina*. Bull. Environ. Contam. Tox. 109, 180-185.

CHENG G., LI Y., ZHANG M., 2022. *Research progress on desulfurization technology of high-sulfur bauxite*. T Nonferr Metal Soc. 32, 3374-3387.

CHENG G., ZHANG J., SU H., ZHANG Z., 2023. *Synthesis and characterization of a novel collector for the desulfurization of fine high-sulfur bauxite via reverse flotation*. Particuology 79, 64-77.

CHENG W., DENG Z., TONG X., LU T., 2020. *Hydrophobic Agglomeration of Fine Pyrite Particles Induced by Flotation Reagents*. Minerals 10, 801.

CHO J., JUNG M.Y., LEE H., AN J., 2022. *Froth-Flotation Separation as an Alternative for the Treatment of Soil Enriched with Fluorine Derived from Mica.* Int. J. Env. Res Pub. Health 19, 1775.

COOK B.K., GIBSON C.E., 2023. *A Review of Fatty Acid Collectors: Implications for Spodumene Flotation*. Minerals 13, 212.

CRUZ N., PENG Y., WIGHTMAN E., XU N. ,2015. *The interaction of pH modifiers with kaolinite in copper–gold flotation.* Miner. Eng. 84, 27-33.

FARROKHPAY S., 2012. *The importance of rheology in mineral flotation: A review*. Miner. Eng. 36-38, 272-278.

FU W., CHEN B., ZHANG K., LIU J., SUN X., HUANG B., SUN B., 2022. *Rheological Behavior of Hydrate Slurry with Xanthan Gum and Carboxmethylcellulose under High Shear Rate Conditions*. Energ. Fuel 36, 3169-3183.

FU Y., YIN W., DONG X., SUN C., YANG B., YAO J., LI H., LI C., KIM H., 2021. *New insights into the flotation responses of brucite and serpentine for different conditioning times: Surface dissolution behavior*. International Journal of Minerals, Metallurgy and Materials 28, 1898-1907.

HAN F., PU S., ZHOU Y., ZHANG H., ZHANG Z., 2022. *Effect of ultrafine mineral admixtures on the rheological properties of fresh cement paste: A review*. Journal of Building Engineering 51, 104313.

HU P., LIANG L., 2020. *The role of hydrophobic interaction in the heterocoagulation between coal and quartz particles*. Miner. Eng. 154, 106421.

JIN D., SUN R., WANG G., DENG J., ZHANG X., 2023. *Flotation separation of fluorite and calcite using anhydrous glucose and aluminum sulfate as a combined depressant*. Appl. Surf. Sci. 624,157089.

KUMAR K., ARORA R., 2022. *Effect of additive on rheology of fine particles slurry suspension*. Materials Today: Proceedings 50:1413-1416

LAHIRU B., NIMAL S., BORIS A., 2017. *Influence of clays on the slurry rheology and flotation of a pyritic gold ore.* Appl. Clay. Sci. 136, 230-238.

LI H., CHAI W., CAO Y., YANG S., 2022. *Flotation enhancement of low-grade bauxite using oxalic acid as surface pretreatment agent.* Appl. Surf. Sci. 577, 151964.

LIU C., DENG J., NI C., WANG D., XUE K., XU L., ZHANG X., 2022. *Reverse froth flotation separation of limonite and quartz with cationic gemini surfactant.* Miner. Eng. 177, 107391.

LIU D., ZHANG G., GAO Y., 2021. *New perceptions into the detrimental influences of serpentine on Cu-Ni sulfide flotation through rheology studies and improved the separation by applying garnet.* Miner. Eng. 171, 107110.

MAMEDOV V., BOEVA N., MAKAROVA M., SHIPILOVA E., MELNIKOV P., 2022. *The Problem of the Formation of Boehmite and Gibbsite in Bauxite-Bearing Lateritic Profiles.* Minerals 12, 389.

OWUSU C., FORNASIERO D., ADDAI-MENSAH J., ZANIN M., 2015. *Influence of pulp aeration on the flotation of chalcopyrite with xanthate in chalcopyrite/pyrite mixtures.* Int J Miner Process 134, 50-57.

SAJJAD M., OTSUKI A., 2022. *Correlation between Flotation and Rheology of Fine Particle Suspensions.* Metals 12, 270.

SANEIE R., ABDOLLAHI H., GHASSA S., AZIZI D., CHEHREH CHELGANI S., 2022. *Recovery of Copper and Aluminum from Spent Lithium-Ion Batteries by Froth Flotation: A Sustainable Approach.* Journal of Sustainable Metallurgy 8, 386-397.

SHAIKH S., STREDNAK S., BUTLER J.E., 2022. *Advances in the Rheological Characterization of Slurries of Elongated Particles.* Kona Powder Part. J. 39, 84-99.

SHAO X., WU G., JIANG G., WANG Y., PU S., LAN Y., JIANG D., 2023. *Effect of La Doping and Al Species on Bastnaesite Flotation: A Density Functional Theory Study.* Minerals 13, 583.

SULLIVAN J.P., BOSE A., 2022. *On the connection between slurry rheology and electrochemical performance of graphite anodes in Lithium-ion batteries.* Electrochem. Commun. 141, 107353.

SUN Q., WANG S., MA X., ZHONG H., 2021. *Desulfurization in high-sulfur bauxite with a novel thioether-containing hydroxamic acid: Flotation behavior and separation mechanism.* Sep. Purif. Technol. 275, 119147.

WANG D., LIU Q., 2021. *Influence of aggregation/dispersion state of hydrophilic particles on their entrainment in fine mineral particle flotation.* Miner. Eng. 166, 106835.

WANG M., ZHU Z., LIU R., LI S., ZHANG C., LIU Y., ZHANG L., BAI J., 2021. *Influence of extreme high-temperature environment and hydration time on the rheology of cement slurry.* Constr. Build. Mater. 295, 123684.

WANG N., LU J., YIN W., YAO J., 2022. *Innovative flotation for the utilisation of carbonate-bearing (siderite) iron ore using MS-2 as a dispersant.* Powder Technol. 399, 116989.

WESTON J.S., CHUN J., SCHENTER G., WEIGANDT K., ZONG M., ZHANG X., ROSSO K.M., ANOVITZ L.M., 2020. *Connecting particle interactions to agglomerate morphology and rheology of boehmite nanocrystal suspensions.* J. Colloid Interf. Sci. 572, 328-339.

WU H., LI J., CHEN C., XIA F., XIE Z., 2020. *Suspension calcination and alkali leaching of low-grade high-sulfur bauxite: Desulfurization, mineralogical evolution and desilication.* International Journal of Minerals, Metallurgy and Materials 27, 602-610.

XIAO W., SHAO Y., YU J., ZHANG B., SHU H., ZHANG Y., 2022. *Activation of ilmenite flotation by Al^{3+} in the benzohydroxamic acid (BHA) system.* Sep. Purif. Technol. 299, 9.

YANG L., ZHU Z., LI D., YAN X., ZHANG H., 2019. *Effects of particle size on the flotation behavior of coal fly ash.* Waste Manage 85, 490-497.

ZHANG F., LU Y., HAN F., WEN G., GU S., TANG P., 2022. *Effect of ball-milling parameters on the rheological properties of mold powder slurry.* Ceram. Int. 48, 14192-14200.

ZHANG H., ZHOU F., YU H., LIU M., 2021. *Double roles of sodium hexametaphosphate in the flotation of dolomite from apatite.* Colloids and Surfaces A: Physicochemical and Engineering Aspects 626, 127080.

ZHANG M., PENG Y., 2015. *Effect of clay minerals on pulp rheology and the flotation of copper and gold minerals.* Miner. Eng. 70, 8-13.

ZHANG P., JIN S., OU L., ZHANG W., ZHU Y., 2020. *Fine Bauxite Recovery Using a Plate-Packed Flotation Column.* Metals 10, 1184.

ZHANG P., ZUO L., WANG Y., SUN X., LIU R., LIU L., MA Y., 2023. *Nanogeochemistry of karst-type bauxite from Jingxi, Guangxi, China: Revealing a new occurrence of Al, Si, Ti, Fe, and C by nanoparticles in karst-type bauxite deposit.* Ore Geol. Rev. 157, 105449.

ZHANG X., ZHANG X., LI X., MA M., ZHANG Z., JI X., 2023. *Slurry rheological behaviors and effects on the pore evolution of fly ash/metakaolin-based geopolymer foams in chemical foaming system with high foam content*. Constr. Build. Mater. 379, 131259.

ZHANGLEI Z., DONGHUI W., BIN Y., WANZHONG Y., MORTEZA S.A., JIN Y., JAROSLAW W.D., 2020. *Effect of nano-sized roughness on the flotation of magnesite particles and particle-bubble interactions*. Miner. Eng. 151.

ZHAO B., CHEN Y., JIU S., 2021. *Effective Desulfurization and Alumina Digestion of High-Sulfur Bauxite by New Roasting Process with Conveying Bed*. Processes 9, 390.

ZHOU H., XU L., WANG D., XUE K., TIAN J., 2023. *Selective adsorption mechanism of SHMP onto fine fluorite in bastnaesite flotation system.* Colloids and Surfaces A: Physicochemical and Engineering Aspects 670, 131527.

ZHOU J., MEI G., YU M., SONG X., 2022. *Effect and mechanism of quaternary ammonium salt ionic liquid as a collector on desulfurization and desilication from artificial mixed bauxite using flotation*. Miner. Eng. 181, 107523.

ZHOU X., YIN J., CHEN Y., XIA W., XIANG X., YUAN X., 2018. *Simultaneous removal of sulfur and iron by the seed precipitation of digestion solution for high-sulfur bauxite.* Hydrometallurgy 181, 7-15.